460 KSME Journal, Vol. 8, No. 4, pp. 460~474, 1994

Experiments on the Turbulent Shear Flow in a Turn-Around Duct(II) — The Structure of Turbulence

Jung-Chul Shin*

(Received March 16, 1994)

Detailed measurements including two-component mean velocities(U and V), RMS of turbulent fluctuations(u' and v') and turbulent cross-correlation($u'v'$) were made throughout a turn-around duct. Two-component velocity data were obtained using a Laser Doppler Velocimeter. With the aid of a digitized data acquisition system, energy spectra were estimated using a Fast Fourier Transform. Along the outer wall, the flow is affected more than the half across the channel height due to the centrifugal instability. The measured results are consistent with the turbulence production mechanism for stabilizing and destabilizing curved flows. Energy production and dissipation are reduced along the convex wall and amplified along the concave wall. In the quasi-laminar region, turbulent fluctuations and cross-correlations are damped. The mean flow and turbulence structure in this region are influenced mainly by the streamwise pressure gradient rather than curvature. The flow in the downstream part of the turn is dominated by the inertial effect. The turbulent large eddy motions along the concave wall are strongly anisotropic.

Key Words: Curved Flow Turbulence, Turbulent Intensity, Turbulent Shear Stress, Turbulert Energy Spectra, Curved Flow Stability, Fourier Transform, Turbulent Energy Equation

1. Introduction

The Bradshaw's analogy(1969) between streamline curvature and buoyancy in turbulent shear flow, which has been used by many investigators in the mildly curved flows, may not be adequate for the strongly curved flows. Detailed turbulence structure on a mildly curved convex surface was studied by Muck et al.(1985). Turbulent quantities, skewness and flatness factors were measured and the turbulent kinetic energy balance was evaluated. The dissipation term was evaluated from the energy balance. They concluded that the response of the boundary layer upstream to the curvature is faster along the convex wall than the concave wall. Using the same test facility, Hoffmann et al.(1985) investigated the effect of concave surface curvature. Since naturally occuring vortices were small on the concave surface, they introduced artificial disturbances to trigger a steadier and more regular vortex pattern. Spanwise variation of the streamwise mean velocity and skin friction coefficient was measured. Also, detailed turbulence structure including triple products were measured. They suggested that if the curvature is moderate, the percentage spanwise variation of surface shear and heat transfer rate is very small. This small variation of surface shear was also confirmed by Barlow and Johnston(1988). Smits et al. (1979) have evaluated the effects of short fetches of both convex and concave curvature. The high Reynolds stresses near the turn exit along the concave wall did not decay monotonically in the downstream recovery section; they were still falling slowly at the end of the test rig, although they must recover eventually. However, on the convex side the flow recovers monotonically from the low level of

* Korea Atomic Energy Research Institute

Reynolds stresses near the turn exit. For constant pressure gradient flow along the convex wall, the turbulence virtually disappeared in the outer layer and was obviously decreased in the inner layer (So et al., 1972). Gillis and Johnston(1983) have studied the effect of convex curvature only, and produced a zero streamwise pressure gradient by modifying the outer concave wall geometry. The flow from a flat surface was passed over a convex surface with 90° of turning and then onto a flat recovery surface. They confirmed So and Mellor's(1972) results that, after the sudden introduction of curvature, the shear stress in the outer part of the boundary layer is sharply diminished and recovers very slowly towards the flat plate condition downstream. The entrainment rate is reduced by the curvature and remains low all the way through the recovery section. Wilcken(1930) and Wattendorf(1935) showed that the mixing length models for the turbulent shear stress are not adequate for the curved flow.

Previous experimental facilities for curved turbulent flow are compared to the present facility as listed in Table 1. The present turn-around duct model has both a larger curvature and a higher Reynolds number. Based on the present measured results, an analysis of the response of turbulent boundary layers to the occurrence of an abrupt

Table 1 Comparison of experimental facilities for curved turbulent flow

Reference	Aspect Ratio b/h	Turning Angle (deg.)	$\frac{\delta_i}{R}$	$\frac{h}{R_m}$	$\frac{L_1}{\delta_i}$	$\frac{L_2}{\delta_i}$	Re
Wilcken(1930)	6.5	180	0.25	0.67	40	0	$U_m h/\nu = \frac{80{,}000}{103{,}000}$
Wattendorf(1935)	18.0	300	0.125	0.22	114	0	$U_m h/\nu = \frac{27{,}000}{80{,}000}$
Eskinazi and Yeh(1956)	15.5	300	0.045	0.087	64	0	$U_m h/\nu = 148{,}000$
So and Mellor(1972)	8.0	150	0.08	0.46	48	0	$U_\infty \delta_i/\nu = 36{,}400$
Ellis and Joubert(1974)	13.2	360	0	0.17	0	0	
Meroney and Bradshaw(1975)	6.0	28	0.01	0.051	58	0	$U_\infty \delta_i/\nu = 52{,}000$
Ramaprian and Shivaprasad	2.5	33	0.013	0.04	61.5	0	$U_\infty \delta_i/\nu = 28{,}500$
Hunt and Joubert(1979)	13.2	43	0	0.01	0	0	$U_m h/\nu = \frac{30{,}000}{130{,}000}$
Smit et al.(1983)	6.0	30	0.17	0.67	66	66	$U_\infty \delta_i/\nu = 44{,}000$
Gillis et al.(1985)	6.7	90	0.09	0.29	64	24	$U_\infty \delta_i/\nu = 48{,}000$
Hoffmann, Muck and Bradshaw	6.0	28	0.01	0.051	58	0	$U_\infty \delta_i/\nu = 56{,}000$
Present Study	10.0	180	0.3	1.0	62.5	21.3	$U_m h/\nu = \frac{70{,}000}{500{,}000}$

δ_i : Boundary Layer Thickness at the inlet of curved section, L_1 : Inlet Length, L_2 : Downstream Recovery Length, b : Channel Span Length, h : Channel Height, R_m : Mean Radius, R : Radius of the Wall.

curvature was made in this study. An inner convex wall flow and an outer concave wall flow were evaluated by examining the streamwise development of turbulent fluctuations as well as turbulent shear stresses. The structure of turbulence was also studied.

2. Experimental Works

The test facility is the same as the Part-(I)-The mean flow characteristics. The turn-around duct model was constructed with the thick lucite through which the Laser Doppler Velocimeter(LDV) could be operated. The aspect ratio of the test section, b/h, is 10.0 where b is the channel span and h is the channel height. Lake water located above the test facility comes directly into the entrance of the test section. The flow rate was controlled by a 0.61 m control valve located upstream from the test section. A digital computer combined with an analog to digital board was used to read the output signal and to reduce the experimental data. Two-component velocity data, turbulent shear stress, surface shear stress and time series data were obtained from the digitized output signals. Most of data processing were performed by suitable FORTRAN programs.

Two-component velocity measurements near the wall were less accurate than in the core region because the beams are limited in rotation, thus the sensitivity to the flow in the vertical direction is small.

Errors in LDV measurements have been discussed by Durst et al.(1976) and McLaughlin and Tiederman(1973). According to their study, the systematic errors were attributed mainly to velocity bias, mean velocity gradient broadening, finite transit time broadening and instrument noise broadening. Broadening causes an increase in the RMS of the doppler frequency over that of the true velocity distribution. For the present experiment, the natural particles are uniformly distributed in the testing water and an accurate analysis of the biasing error is difficult. The biasing error may be estimated from the results of McLauglin and Tiederman(1973). The region near the concave wall the intensities are lower than 20% for which the corresponding biasing error is of the order of 3%. In the present study it was assumed that the biasing error correction was of negligible importance. No corrections were made for finite transit time broading in this study. For the conditions of this study, velocity gradient broadening was estimated to be significant only immediately adjacent to the channel surface. The instrument noise broadening effects were found to be small and not important over most of the flow field.

The uncertainty analysis described by Kline and McClintock(1953) was employed in the present study in order to estimate the error range due to random errors. The error range of output signals which was used as a base of the uncertainty evaluation for the results, was obtained by repeated measurements at a given point. These maximum uncertainties observed from the direct measurements are given in Table 2. The estimated uncertainties for the results are tabulated in Table 3.

The output signals were stored on computer disks for time series analysis. The auto-

Table 2 Maximum uncertainty observed

Signal processor	
$W(E)/E$	0.30%
$W(\overline{e^2})/\overline{e^2}$	4.85%
Angle change, $W(\beta)$	0.50
Pressure transducer	
$W(E)/E$	4.50%

Table 3 Estimated maximum uncertainty

$W(U)/U$	0.30%
$W(V)/V$	2.44%
$W(u')/u'$	2.43%
$W(v')/v'$	6.05%
$W(\overline{uv})/\overline{uv}$	7.32%
$W(\Delta P)/\Delta P$	5.10%
$W(\tau_w)/\tau_w$	10.4%
Flow angle, α	0.478

correlation function of u at a given point is defined by,

$$\hat{R}_{11}(t)=\lim_{T\to\infty}\frac{1}{T}\int_0^T u(\tau)u(\tau+t)d\tau \qquad (1)$$

where T is a sample period and t is a time lag. The one-dimensional energy spectra of u, $\hat{E}_{11}(k_1)$, is defined as,

$$\int_0^\infty \hat{E}_{11}(k_1)dk_1=\overline{u^2} \qquad (2)$$

where k_1 is the wave number in the x-direction. If the frequency domain is used for representing the energy distribution, the relation, $k_1=2\pi f/U$ gives the frequency spectra, $\hat{F}_{11}(f)$,

$$\int_0^\infty \hat{F}_{11}(f)df=\overline{u^2}$$

$$\text{where } \hat{F}_{11}(f)=\frac{2\pi}{U}\hat{E}_{11}(k_1) \qquad (3)$$

The frequency spectra were first calculated by the standard Fast Fourier Transform(FFT) method described in Bendat and Piersol(1971). And then the auto-correlation function was obtained by the inverse Fourier Transform of the frequency spectra, since the two functions are Fourier Transform pairs.

The computed auto-correlation fuction obtained from the inverse Fourier Transform of the spectra was compared to the direct computed auto-correlation function, estimated by the following discrete form,

$$\hat{R}_{11}(i\Delta t)=\frac{1}{N-1-i}\sum_{j=0}^{N-1-i}X_jX_{j+i},$$

$$i=0,\ 1,\ 2,\ \cdots,\ M \qquad (4)$$

where $i\Delta t$ is a time lag and M is a maximum lag number. In general M is much smaller than the sample size, N. Figure 1 shows the comparison of two different computation of the auto-correlation coefficient, $R_{11}(t)=\hat{R}_{11}(t)/\overline{u^2}$. The input data were taken at the 17.3 cm upstream of the turn with $y/\delta=0.15$. Although the large time lag deviates slightly, the region determining the integral time scale are almost the same. Slight deviation in the large time lags indicates that the calculated spectral curve at the lowest frequencies using FFT may not be accurate. However the error does not seem to be significant as seen in

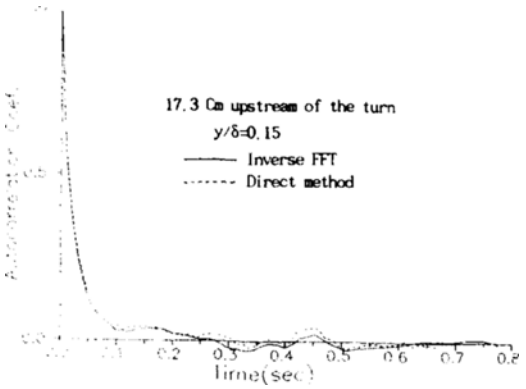

Fig. 1 Comparison of autocorrelation coefficient between inverse FFT and direct method

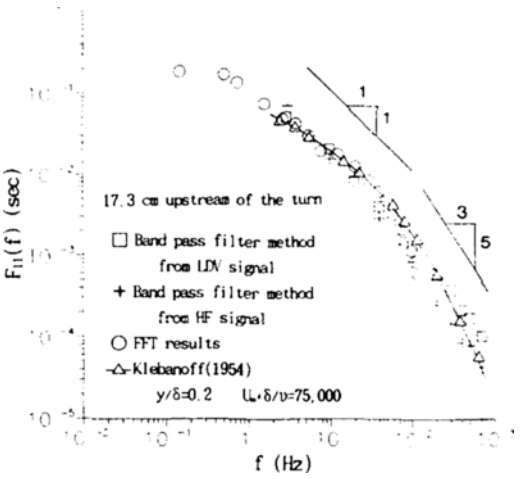

Fig. 2 Comparison of frequency spectra of u over the flat wall upstream of the turn.

Fig. 2, in which the computed spectra is compared with Klebanoff's experimental results for a zero pressure gradient flow over a flat wall. The spectral results in this figure were represented in the wave number domain and normalized by $\overline{u^2}$, $E_{11}(k_1)=\hat{E}_{11}(k_1)/\overline{u^2}$. The input data is the same as the one represented in Fig. 1 before. It shows that the cut off frequency (equivalent to $k_1=3.13$ cm^{-1}) of the present spectral data limits the high frequency information. However, the energy containing range(-1 slope) shows good agreement with Klebanoff's(1954) measurement. The validity of the FFT program was checked by comparing the measured RMS value to the value

obtained from the integration of the computed frquency spectra curve. The direct measurement of frequency spectra using an analog spectrum analyzer was also performed in this study. Figure 2 shows the comparison of the FFT results with the analog measured frequency spectra from both LDV and Hot Film. The normalized spectra were taken at the center of Station 5 for the low Re flow. The laser velocimeter data agree with the anemometer results up to about 100 Hz. The good agreement between the two independent measuring systems LDV and Hot Film indicated that external particle control was unnecessary. The deviation of the laser measurements at high frequencies do not affect the RMS values of the fluctuations since most of the contributions to the RMS values come from frequencies less than 100 Hz. The deviation above 100 Hz is partly due to ; the failure of the larger particles in the flow to follow the high frequency fluctuations, the velocity fluctuations within the scattering volume and the finite volume effect mentioned before. The LDV results show the broadening of the turbulent energy in the high frequency range, which is inherent in LDV measurements. From the spectral results, it was determined that a low-pass filter should be used to limit the high frequency range for the velocity measurements.

3. Flow Along a Convex Wall

Near the start of the turn along the inner wall the turbulent fluctuations as well as viscous effects are greatly reduced due both to the streamwise favorable pressure gradient and to the stabilizing convex curvature. The turbulence receives its energy from the mean motion and finally dissipates it through the action of molecular viscosity transport. So and Mellor(1972) derived the turbulent energy equations in curvilinear coordinates. Without boundary layer approximations, the following production terms can be extracted from the complete equations.

$$\frac{1}{2}u^2 : -\frac{u^2}{1+ky}\frac{\partial U}{\partial x} - \underline{uv\frac{\partial U}{\partial y}} - uv\frac{kU}{1+ky} - \underline{\frac{3u^2}{2}\frac{kV}{1+ky}} \tag{5a}$$

$$\frac{1}{2}v^2 : -v^2\frac{\partial V}{\partial y} - \underline{\frac{uv}{1+ky}\frac{\partial V}{\partial x}} + uv\frac{2kU}{1+ky} - \frac{v^2}{2}\frac{kV}{1+ky} \tag{5b}$$

$$\frac{1}{2}w^2 : -\frac{w^2}{2}\frac{kV}{1+ky} \tag{5c}$$

$$\frac{1}{2}q^2 : -\frac{u^2}{1+ky}\frac{\partial U}{\partial x} - v^2\frac{\partial V}{\partial y} - uv\left(\frac{\partial U}{\partial y} + \frac{1}{1+ky}\frac{\partial V}{\partial x} - \frac{kU}{1+ky}\right) - \frac{(3u^2+v^2+w^2)}{2}\frac{kV}{1+ky} \tag{5d}$$

$$-uv : v^2\frac{\partial U}{\partial y} + \frac{uv}{1+ky}\frac{\partial U}{\partial x} + \frac{u^2}{1+ky}\frac{\partial V}{\partial x} + uv\frac{\partial V}{\partial y} - (2u^2-v^2)\frac{kU}{1+ky} - uv\frac{2kV}{1+ky} \tag{5e}$$

The effect of curvature is reflected by the terms containing k in the above quantities. The normal mean velocity, V, is negative near the start of the turn. Although V exists in this region, the present measurement shows that V, $\partial V/\partial x$ and $\partial V/\partial y$ (except very near the surface) are one order of magnitude smaller than U, $\partial U/\partial x$ and $\partial U/\partial y$. The underlined terms were assumed to be the most important terms for energy production(as a first order approximation). The term $uvkU/(1+ky)$ in Eq. (5d) is negative for $uv > 0$, since k is positive for the convex wall flow. Apparently the turbulent energy is absorbed, not frozen, by the curvature forces. Moreover if the flow accelerates in the x-direction, the first term in Eq. (5d) contributes more to reduce the production of the turbulent energy, which does not appear for the curved flow without pressure gradient. Equation (5e) shows that $-uv$ decreases if $2u^2 > v^2$; the decrease is greater when the flow accelerates, since the second term in Eq. (5e) contributes negatively. The production of v^2 is suppressed for the convex wall flow without a pressure gradient. According to the rapid distortion theory, however, v^2 increases and u^2 decreases due to the contraction of the stream tube if the curvature does not exist. The behavior of v^2 is considered to depend on the degree of curvature and streamwise pressure gradient. For the convex wall flow without pressure gradient the production of u^2

increases according to the third term in Eq. (5a). For the present flow, however, the first term dominates due to strong streamwise pressure gradient and in addition, $u^2 > -\overline{uv}$ so that a reduction of $\overline{u^2}$ occurs. In conclusion, the energy production and turbulent shear stress as well as the energy transport are reduced in the convex wall flow.

4. Flow Along a Concave Wall

The production mechanism for a concave wall flow is, in general, opposite to the one for a convex wall flow since k is negative. $q^2(=u^2+v^2+w^2)$ in Eq. (5d) increases due in part to the concave surface and in part to the adverse pressure gradient near the inlet of the turn. The fifth term in Eq. (5e) contributes positively only if $2u^2 > \overline{v^2}$ or $v'/u' < 1.414$. However the second term accelerates the increase of $-\overline{uv}$. From Eqs. (5a) and (5b), $\overline{v^2}$ is clearly excited by the curvature forces while $\overline{u^2}$ increases if $|u^2 \partial U/\partial x| > |uv\,kU|$. Different from the plane flow, Margolis and Lumley(1965) found experimentally that in a curved mixing layer (Max. $\delta/R = 0.2$) the dominant terms in the turbulent energy balances for a concave wall flow are the production and the diffusion by the turbulent velocities. Compared to the mildly curved flow, much larger turbulent kinetic energy diffusion flux occurs toward the outer region in the present flow due to the strong curvature. Thus $\overline{u^2}$ is expected to be larger, due to the turbulent diffusion. Opposite to the convex wall flow, the turbulent energy production and turbulent shear stress as well as the turbulent energy transport are enhanced for the concave wall flow.

5. Results and Discussion

5.1 Streamwise developments of turbulence intensity and turbulent shear stress

The flow upstream is not yet fully developed but close to the results for developing flow reported by Barbin and Jones(1963). Isometric plots of the streamwise variations of u'/U_m, v'/U_m and $\overline{uv}/U_m^2$ around the turn are shown on Figs. 3, 4 and 5; and detailed values appear on Figs. 6 through 11. U_m is the average velocity across the channel height at the inlet of the test section. It is noted that v' and $\overline{uv}$ were not measured very near the wall($y/h \leq 0.04$) and therefore the lines near the wall in the isometric figures were extrapolated smoothly to the wall. However the general behaviors of v' and $\overline{uv}$ are well described in their isometric plots. The present measurements show that u^2, v^2, and $\overline{uv}$ are diminished along the convex wall and greatly enhanced along the concave wall due to the curvature effect and to the streamwise pressure gradient effect. The adverse streamwise pressure gradient promotes the turbulent mixing while the favorable pressure gradient dampens the turbulent motions. It is recalled from the Part-(I) that along the concave wall the streamwise pressure gradient is almost constant between 50° and 130° around the turn, while along the convex wall the constant pressure gradient region is nearly absent. One of the new observations is that v^2 increases greater than u^2. The turbulent fluctuations and momentum exchange in the normal direction are more promoted by the curvature than that in the streamwise direction. As seen before the production mechanism indicates that v^2 increases due to curvature effects while the increase of u^2 is due to the decelerating flow near the start of the turn. Different from u', therefore, v' increases continuously as the flow travels along the concave wall. The v^2 is higher than uv along the concave wall although uv increases greatly, as seen in Fig. 5. Higher turbulence intensities and turbulent cross-correlation occur in the downstream recovery section, compared to the turn inlet. This high turbulence level persists throughout the straight exit section, which is consistent with previous observations. Due to much higher turbulent fluctuations in the downstream recovery section, compared to the upstream inlet level before the turn, the recovery length could appreciably affect the pressure loss throughout the curved channel.

5.1.1 Turbulent fluctuations

Along the concave wall the higher intensity level compared to the flat wall flow upstream was caused partly by the adverse pressure gradient

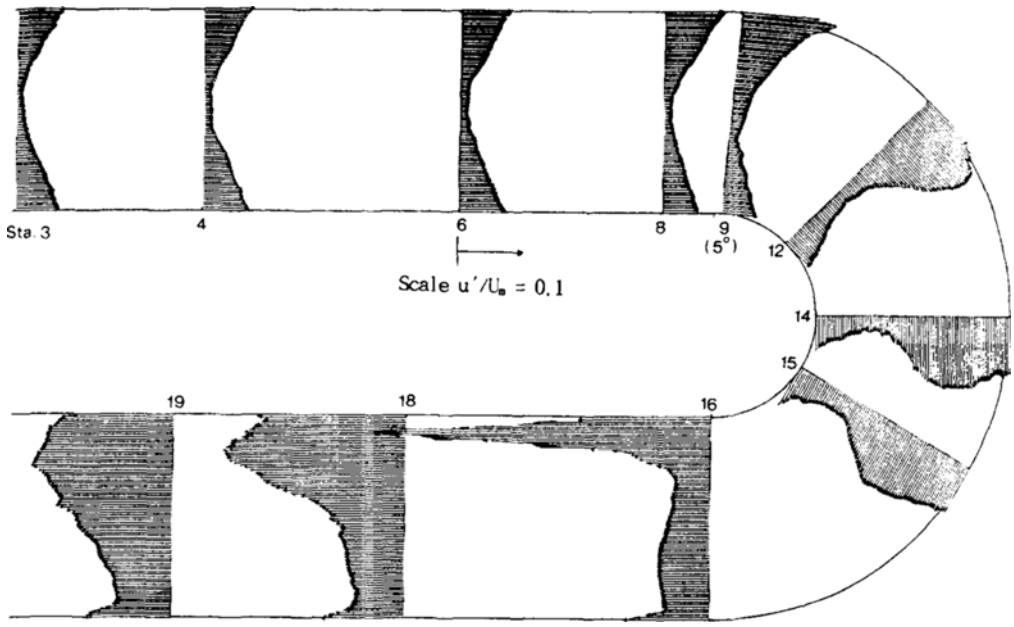

Fig. 3 Streainwise turbulence intensity changes through the turn-around duct

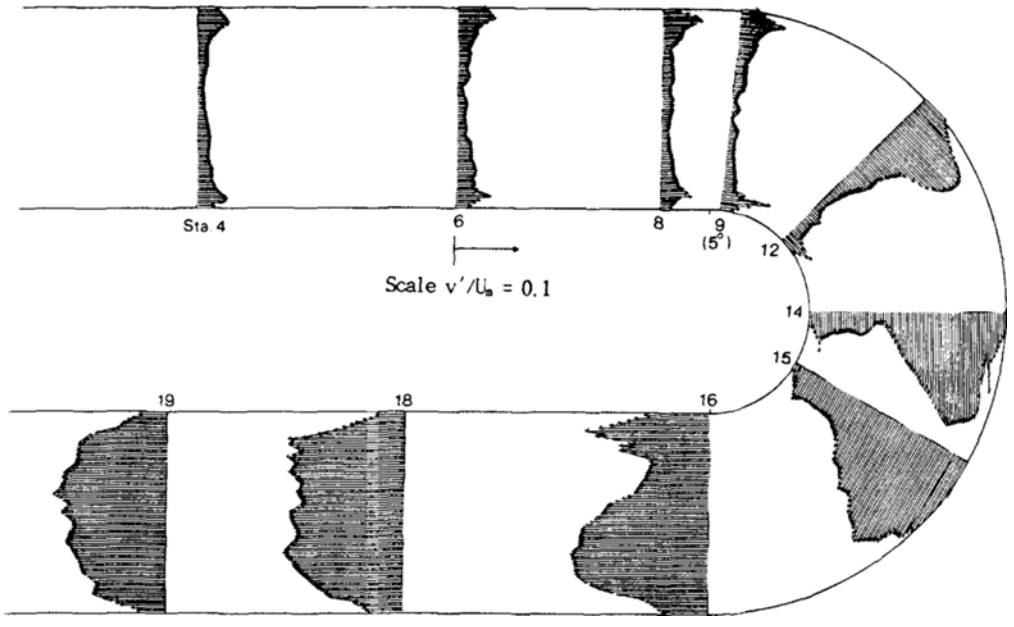

Fig. 4 Vertical turbulence intensity changes through the turn-around duct

near the start of the turn and by the destabilizing concave curvature. As the flow travels along the concave wall the maximum intensity point moves away from the wall and the u' distributions tend to spread out over a large portion of the boundary layer as seen in Fig. 6. This behavior is also observed for v' and $\overline{uv}$. It appears that the turbulent energy is diffused from the inner region to the outer region. It is unrealistic that a maximum in u'/U_m occurs very near the wall where the data

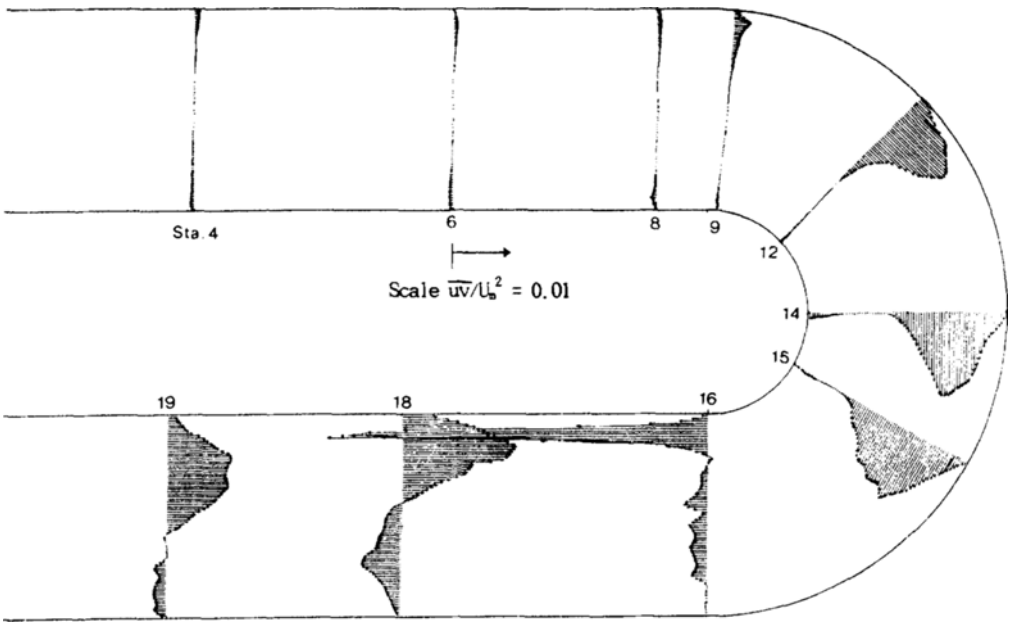

Fig. 5 Turbulent shear stress changes through the turn-aroun duct

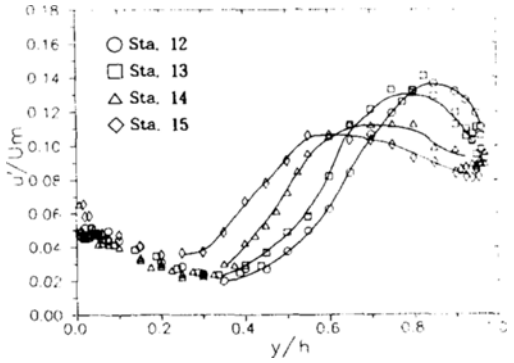

Fig. 6 Streamwise turbulence intensities in the turn

could not be obtained. As previous investigators indicated, the curvature affects the flow mostly in the outer shear layer rather than in the inner layer(So et al., 1972; Ramaprian et al., 1978; Hunt et al., 1979), so that the inner layer changes little. u' decreases slightly once the turn exit is reached.

Along the concave wall, v' greatly increases compared to u', approaching $v'/u'=1.8$ in the downstream part of the turn. This indicates that the turbulent large eddy motions along the concave wall are strongly anisotropic. The continuous increase of v'/u' reaches a maximum value of 2.6 at the exit of the turn, showing v' is more affected by the concave curvature than u'. The anisotropy for the present flow is also shown in Fig. 12. The spanwise turbulence intensity, w'/U_m, at 90° around the turn along the concave wall was measured independently using a hot film. w' is approximately the same as v' between $y/h=0.65\sim0.85$ for Re ranging from 200,000 to 450,000. However near the wall and in the center region, w' is much higher than u' and v', especially for the high Re flows. The higher value of w' near the wall agrees with So and Mellor's result(1972) but their value of w' in the outer layer was similar to v'. Figure 12 supports the concept that the highly time dependent, non-stationary longitudinal vortices exist along the concave wall. The larger values of w' near the boundary layer edge(central part) and near the wall suggest that a vortex motion exists in the y-z plane. Although the Taylor-Görtler vortices affect the turbulence structure indirectly, their effect would be much smaller than the centrifugal instability effect. The stationary pattern of Taylor-Görtler vortices were not observed for the present flow while much more turbulent fluctuations occur compared to the previously reported,

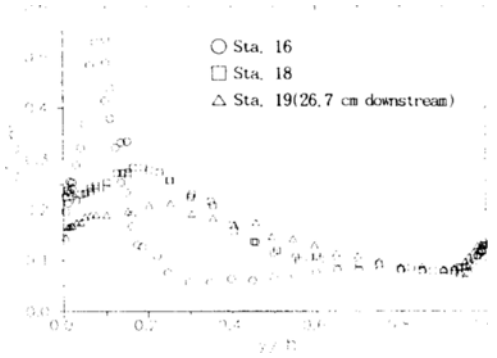

Fig. 7 Streamwise turbulence intensities along the flat wall downstream of the turn

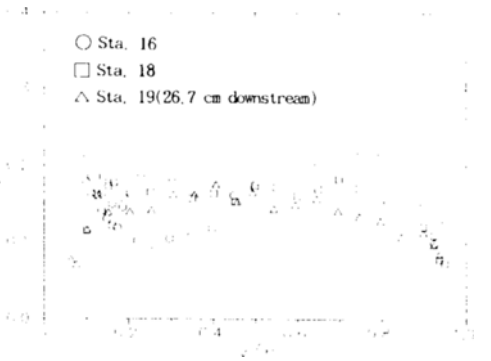

Fig. 9 Normal turbulence intensities along the flat wall downstream of the turn

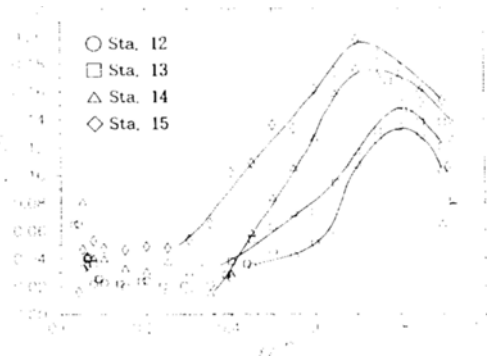

Fig. 8 Normal turbulence intensities in the turn

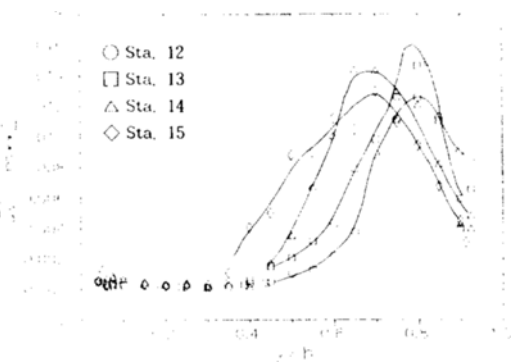

Fig. 10 uv/U_{m2} distributions in the turn

mildly curved flows. It was found that the turbulent kinetic energy increases greatly along the concave wall and decreases along the convex wall. Along the concave wall the energy increases in the turn as indicated by the greater areas under the curves. Similar to the u' distribution the maximum point moves away from the concave wall and becomes broader as the flow continues. The energy is continuously supplied toward the core region through the action of turbulent diffusion as well as the production mechanism. However much higher turbulent energy is encountered near the separation region as shown in Fig. 7.

5.1.2 Turbulent shear stresses

The magnitude of uv decreases once the turn exit is reached as shown in Fig. 11. This result is due to the turbulent shear stress transport in this region. Recalling that v' becomes greater than u' near the turn exit, the concave curvature effect on uv (the third underlined term in Eq. (5e) now contributes negatively. Furthermore the favorable pressure gradient occuring in this region contributes negatively(the second underlined term).

Along the inner convex wall the negative values of uv approach zero at 30° around the turn, and thereafter slightly positive values of uv are measured. The positive values of uv continue until the exit of the turn. The positive values of uv were also found in the measurements of Gillis and Johnston(1983) and Smit et al.(1979) for their convex wall flows with zero pressure gradient. Different from the present flow, their small positive values of uv were observed only in a limited region in the outer layer. As the flow approaches the separation region, the positive values of uv becomes high. After some distance downstream of the turn exit(after reattachment), this large positive value of uv changes sign again

and shows a large negative valve of $\overline{uv}$ at Station 18.

The centrifugal instability mechanism can explain the behavior of u' and v' but not directly that of $\overline{uv}$. The turbulent shear stress can also be written $\tau_t/\rho = R_{uv}u'v'$ in which R_{uv} is the turbulent shear stress correlation coefficient, $R_{uv} = -\overline{uv}/u'v'$. When u' and v' increase, $\overline{uv}$ also increases only if R_{uv} remains unchanged. However, even though u' and v' increase, τ_t can decrease if the turbulent fluctuations are less correlated. In other words, the higher values of u' and v' are the necessary conditions for the increase of $\overline{uv}$ but not necessarily sufficient conditions. Typically R_{uv} has a constant value of 0.5 over most of the boundary layer for the zero pressure gradient flow over a flat wall.(Klebanoff, 1954) The present flow shows a similar value at Station 5 along the convex wall. Although R_{uv} is strictly appropriate only for two-dimensional flow, it may be used for a qualitative interpretation of the turbulence structure in the turn. It was found that the turbulent fluctuations are better correlated along the concave wall(Stations 12, 14 and 15), compared to the flat wall, and less correlated along the convex wall.

The increase of negative cross-correlation along the concave wall may be explained from the mean velocity gradient effect. For the turbulent boundary layer flow, the turbulent shear stress generates the turbulent kinetic energy through the mean velocity gradient so that the turbulent fluctuations can continue. Without the mean velocity gradient there can be no mean shear stress and therefore no mean correlation between u and v. It is apparent then that a gradient is necessary to produce $\overline{uv}$ in the boundary layer flow. Consider a mean flow with a positive velocity gradient in the boundary layer. If a fluid particle moves upward($v>0$), it will tend to have a lower mean velocity than that of the other particles in its new surroundings. Therefore a negative fluctuation of u generally occurs($u<0$). Conversely the particle moved downward($v<0$) gives rise to more likely a positive fluctuation of u($u>0$). As a result of either upward or downward movement, the sign of $\overline{uv}$ becomes negative. In fact Brodkey(1974) found experimentally that in the turbulent boundary layer the largest contributions to $\overline{uv}$ are by the 'ejection' mode(u_-v_+, where the subscripts indicate the directional signs) and the 'sweep' mode(u_+v_-), even though the 'inward interaction' (u_-v_-) and the 'outward interaction'(u_+v_+) exist. For the concave wall flow, the negative cross-correlation($\overline{uv}<0$) is enhanced because the positive potential velocity gradient is steeper than that for the flat wall flow. For the same physical reason the negative cross-correlation is suppressed for the convex wall flow since the positive potential velocity gradient is smaller than that for the flat wall flow. For the present flow, however, the suppression of the negative cross-correlation is so strong, due to the rapid curvature and the

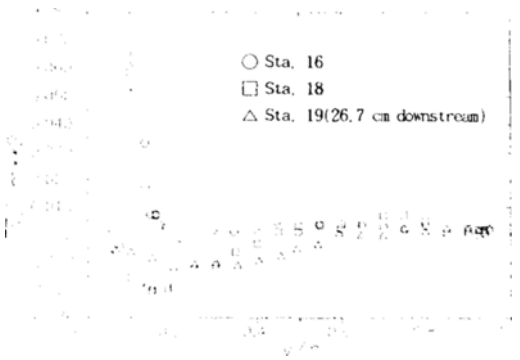

Fig. 11 uv/U_{m2} distributions along the flat wall downstream of the turn

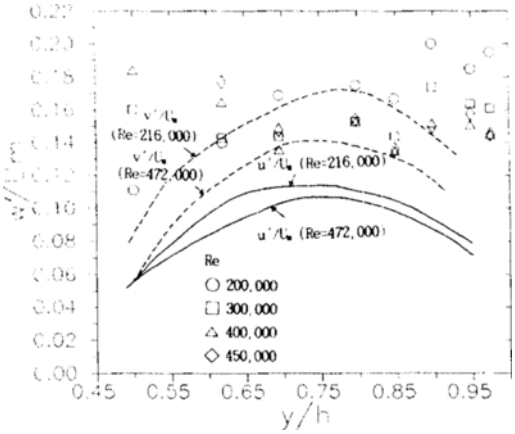

Fig. 12 Spanwise turbulence intensity variations at the 90 deg. around the turn along the outer wall

favorable pressure gradient, that the negative values of $\overline{uv}$ finally die out at approximately 30 ° around the turn along the convex wall, and thereafter positive values of $\overline{uv}$ are measured.

For the present flow, the rate of strain of a fluid element in the x-y plane along the convex wall becomes negative, except very near the wall, due to the strong curvature and the favorable pressure gradient and therefore the sign of $\overline{uv}$ is positive. It is generally acccepted that the turbulent shear stress, τ_t, is related to the rate of strain of the fluid element. Assuming the flow along the convex wall in the central part of the turn is fully developed curved flow with a constant radius, τ_t might be approximated as

$$\tau_t/\rho = -\overline{uv} = \nu_t\left(\frac{\partial U}{\partial r} - \frac{U}{r}\right)$$
$$= \nu_t\left\{r\frac{\partial}{\partial r}\left(\frac{U}{r}\right)\right\} \qquad (6)$$

where ν_t is an eddy viscosity and $\left(\frac{\partial U}{\partial r} - \frac{U}{r}\right)$ is a rate of strain for a curved flow. Since $\partial(U/r)/\partial r$ is negative as shown in Fig. 13, the sign of $\overline{uv}$ must be positive. For comparison, the result of Gillis et al.(1983) for the convex wall flow with zero pressure gradient($\delta/R \simeq 0.09$) is also shown in Fig. 13. They observed small positive values of $\overline{uv}$ for $(r\text{-}R)/\delta > 0.65$. Apparently not only the mean velocity gradient but also the stabilizing convex curvature influences the value of $\overline{uv}$. Their small positive values of $\overline{uv}$ may be due partly to the slight negative values of $\partial(U/r)/\partial r$ near the the boundary layer edge and partly to the turbulent shear stress production along the convex wall. That is, the third underlined term in Eq. (5e) contributes negatively. If the sign of $\overline{uv}$ becomes positive due to the mean velocity gradient effect, this positive value of $\overline{uv}$ increases since the third underlined term arising from the streamline curvature now contributes positively for $2\overline{u^2} > \overline{v^2}$(this inequality is satisfied along the convex wall for the present flow). Furthermore the second underlined term contributes also positively for the positive value of $\overline{uv}$, due to the flow deceleration in the downstream part along the convex wall. Accordingly, both the convex curvature and the adverse pressure gradient contribute to the increase of the positive value of $\overline{uv}$ which has been developed upstream. As a result the high positive values of $\overline{uv}$ are encountered as the flow approachs the turn exit along the inner wall as seen in Fig. 11.

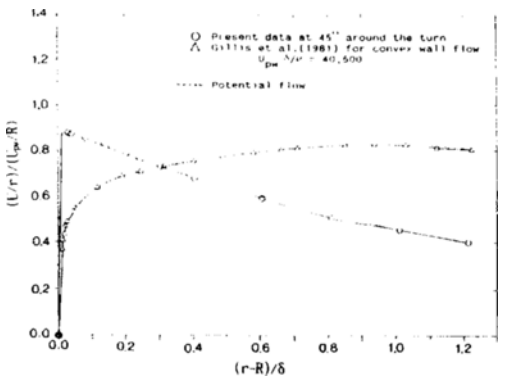

Fig. 13 (U/r)/(U_{pw}/R) profiles in the boundary layer along the convex wall

Near the turn exit along the inner wall(Station 16), the rate of strain($\partial(U/r)/\partial r$) becomes positive for most regions in the shear layer. This result is opposite to the above discussion for the mean velocity gradient effect on $\overline{uv}$. The mean velocity gradient effect on $\overline{uv}$ would be negligible compared to the inertial effect. Higher positive fluctuation of $v(v>0)$ produces more likely a positive fluctuation of $u(u>0)$ in order to satisfy the continuity condition assuming w remain unchanged, while $v<0$ produces $u<0$. Accordingly higher positive cross-correlation is encountered near the turn exit along the inner wall. However after some distance downstream of the turn exit along the inner wall(Station 18), the inertial effect of the flow may be less important compared to the mean velocity gradient effect on $\overline{uv}$. The positive velocity gradient which causes the negative value of $\overline{uv}$ develops after the exit of the turn. After some distance downstream of the turn exit, the negative value of $\overline{uv}$ must be formed in order to recover the normal flat wall flow downstream. After reattachment the negative cross-correlation starts again across the whole boundary layer. Variations of u'/U_m with z/h are within the experimental error as shown in Fig. 14. Hunt and Joubert(1979) investigated the fully

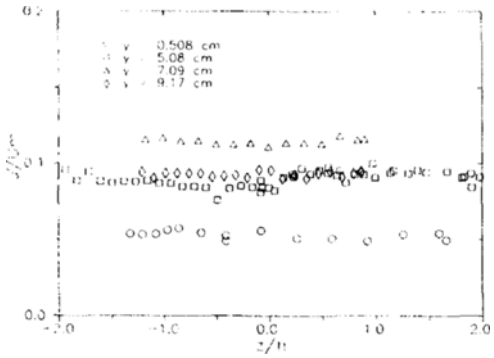

Fig. 14 Spanwise variations of streamwise turbulence intensities at the 90 deg. station

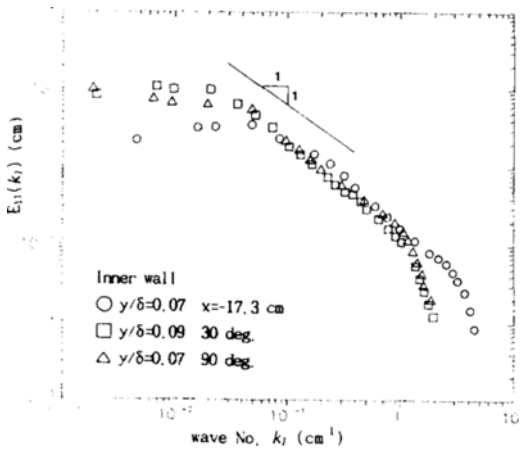

Fig. 15 Energy spectra near the inner layer along the convex wall

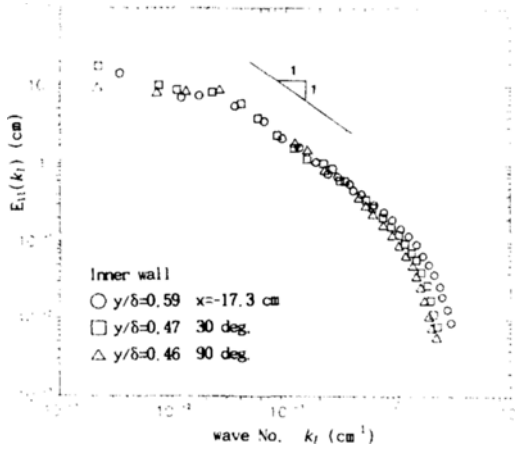

Fig. 16 Energy spectra near the outer layer along the convex wall

developed channel flow in a curved duct with very small curvature $h/R=0.01$. Even for this mild curvature they found significant differences in mean velocities of about 5.5% in the spanwise direction. They found a stationary pattern of Taylor-Görtler vortices in the outer concave wall with the mean spanwise spacing of vortex axis of 0.44 h. The clear appearance of steady Taylor-Görtler vortices found by previous investigators may be a response to fixed upstream disturances.

5.2 Structure of turbulence

For the present flow, the maximum energy containing frequencies (-1 slope region in spectra) were found to be from 3.0 to 8.0 cps across the boundary layer at Station 5. The energy spectra shown in Fig. 15 was taken in the inner layer along the convex wall, a quasi-laminar region. It indicates that in a quasi-laminar region the contribution to energy by larger eddies increases and the small eddy motions are damped. The maximum energy containing wave number decreases from about $k_1=0.24$ cm^{-1}(8 cps) over the flat wall to $k_1=0.06$ cm^{-1}(4 cps) over the curved wall as the flow travels along the inner convex wall. It is noted that the streamwise eddy size can be larger, although u' decreases in this region, since the local mean velocity becomes higher due to acceleration. For the outer layer in this region, Fig. 16, the larger eddy contribution is almost the same as for the flat wall flow. Although deviations in the small eddy motions are observed, their contributions to the turbulent energy is considered to be small.

The contribution to energy by larger eddies in the inner layer along the convex wall is opposite to the results for a mildly curved channel flow reported by Hunt and Joubert(1979) and Ramaprian and Shivaprasad(1978), but consistent with the results for the laminarizing flow over the flat wall by Tanaka and Yabuki(1986). According to the previous investigators for the convex wall flow without acceleration, the larger eddy motion is damped for both the inner and outer layers due to the stabilizing convex curvature. For strongly favorable pressure gradient flow over a flat wall, the integral length scale of u increases due to the

vortex stretching in the streamwise direction and thus streamwise eddy sizes increases. In conclusion, for the present flow the favorable pressure gradient effect overrides the stabilizing convex curvature effect along the convex wall except in the separation region. Due to the onset of curvature, the turbulence structures change quicker in the inner layer than the outer layer, which is consistent with the results of Badrinarayanan and Ramjee(1969) for the strong favorable pressure gradient flow over a flat wall. In the outer layer along the convex wall, the turbulence structures are not yet affected by the curvature as well as the pressure gradient due to the short streamwise distance.

Along the outer concave wall, the energy distributions are almost the same as flat wall flow for the inner layer, Fig. 17. This indicates that the inner layer structure is not influenced by the curvature effect as long as the pressure gradient effect does not exist. This result agrees with earlier findings for curved flow. For the outer layer, Fig. 18, the larger eddy contribution to the energy is almost the same as the flat wall flow. However the small eddy motions tend to decrease although their contribution to the energy is small. This tendency shows a slight evidence that if the curvature continues, the larger eddy motions may be increasing that much since the energy spectra was normalized. For mildly curved flow, earlier researchers found that larger eddy motion is amplified due to the destabilizing concave curvature. Therefore the present flow for both the inner and outer wall does not follow closely the behavior of the fully developed curved flow, but it is processing toward the fully developed condition, which is consistent with the mean flow results.

Figure 19 shows L_x distributions using Taylor's hypothesis along the inner wall in which ψ' is a normalized streamline coordinate. The boundary layer thickness is equivalent to approximately $\psi' = 0.38$ in this region. As expected, L_x at $x = -17.3$ cm becomes smaller as the wall is approached, showing typical boundary layer type flows. As the flow continues along the convex wall, L_x increases for all heights inside the boundary layer. Along the curved section, 30° and 90° around the turn, L_x shows broad profiles across the boundary layer, compared to the data at $x = -17.3$ cm. The flow in the outer layer responds more slowly to the pressure gradient effect than in the inner layer. At the 30° Station, L_x is even greater in the inner layer than the outer layer.

The rate of energy dissipation per unit mass, ε, can be estimated using the relation between and $F_{11}(f)$ in the limited inertial subrange only if the local isotropic assumption is made.

$$\tilde{E}_{11}(k_1) = \alpha' \tilde{\varepsilon}^{2/3} k_1^{-5/3} \tag{7}$$

Due to the limited $-5/3$ slope region in the present spectral curve, the quantity, $\tilde{\varepsilon}$ which imitates the energy dissipation rate, ε was evaluat-

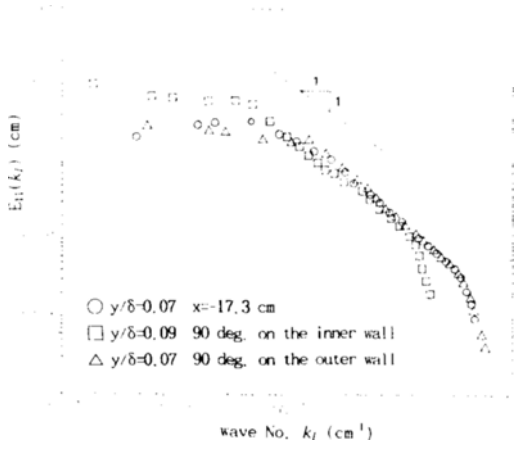

Fig. 17 Energy spectra in the inner layer

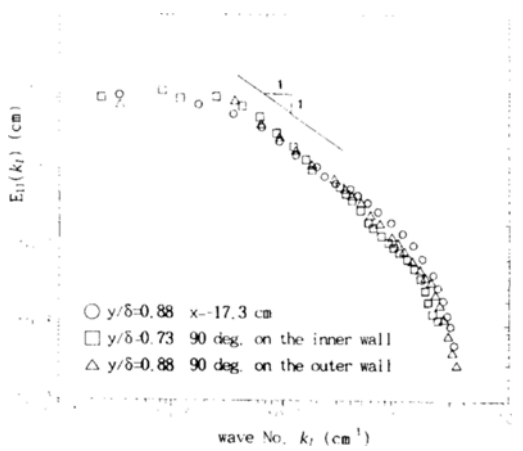

Fig. 18 Energy spectra in the outer layer

ed. The values of $\tilde{\varepsilon}$ could be examined relatively when they are intercompared through the turn as a rough behavior of ε. In a quasi-laminar region $\tilde{\varepsilon}$ is reduced for all height inside the boundary layer due to the reduction of turbulent motion. A decrease of $\tilde{\varepsilon}$ along the convex wall and an increase along the concave wall are consistent with the turbulence production mechanism.

The quantity, $\tilde{\lambda}$ which is a crude approximation of the micro scale was also evaluated from the Taylor's relation, $\varepsilon=15\nu(u^2/\tilde{\lambda}^2)$. It may be used to examine the relative change through the turn. Similar to L_x, the $\tilde{\lambda}$ increases along the inner wall. An increase of L_x and $\tilde{\lambda}$ implies that turbulent eddies are stretched in the streamwise direction due to the contraction of streamline. Both the smaller and larger eddies are affected by the pressure gradient. The increase of L_x and $\tilde{\lambda}$ in a quasi-laminar region is opposite to the convex wall flow without acceleration(Ramaprian et al., 1978). This result again supports the observation that the flow in a quasi-laminar region is more influenced by the pressure gradient effect than the curvature effect. This pressure gradient effect is greater in the inner layer than the outer layer.

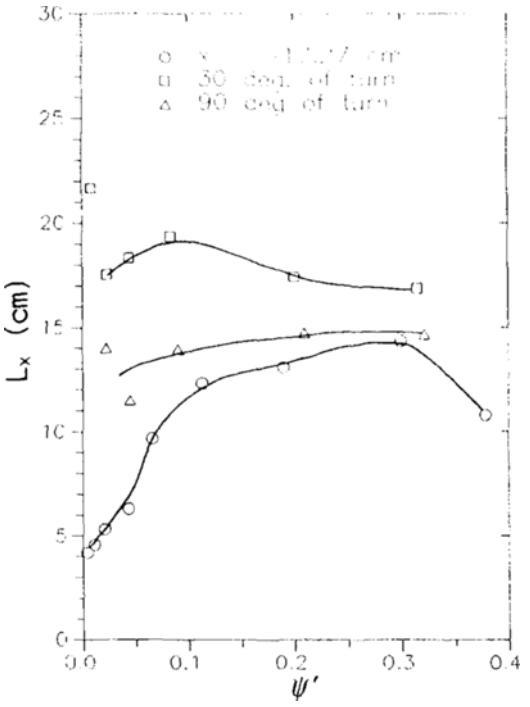

Fig. 19 Turbulence scale distributions along the inner wall.

6. Conclusions

Along the inner convex wall the strain rate of a fluid element becomes negative, except very near the wall, due to strong favorable pressure gradient and convex curvature. Positive values of cross-correlation($\overline{uv}>0$) were measured, which may be due partly to the negative strain rate and partly to the reduction of turbulent shear stress transport in this region. After some distance from the turn exit, the turbulence structure is reorganized passing through the separation region, in order to respond to the positive strain rate developing after the turn exit. Negative values of $\overline{uv}$ were measured after reattachment to recover the flat wall flow downstream. The rate of energy dissipation also greatly increases. Turbulent energy is continuously supplied toward the core region through the action of turbulent diffusion as well as production. The turbulent fluctuations are better correlated for the concave wall flow due to a steeper velocity gradient than the flat wall flow. However, small values of $\overline{uv}$ were encountered near the turn exit along the concave wall, due to the reduction of turbulent shear stress transport in this region. Turbulent fluctuations along the concave wall are not directly coupled with the mean flow. As Reynolds number increases, the turbulent intensities and the turbulent shear stresses decrease.

References

Badrinarayanan, M. A. and Ramjee, A., 1969, "On the Criteria for Reverse Transition in a Two Dimensional Boundary Flow," *J. Fluid Mech.*, Vol. 35, p. 225.

Barbin, A. R. and Jones, J. B., 1963, "Turbulent Flow in the Inlet Region of a Smooth Pipe," *J. Basic Engineering, Trans. ASME*, Vol. 85, p. 29, March.

Barlow, R. S. and Johnston, J. P., 1988, "Structure of Turbulent Boundary Layer on a Concave Surface," *J. Fluid Mech.*, Vol. 191, p. 137.

Bendat, J. S. and Piersol, A. G., 1971, "Random Data : Analysis and Measurement Procedures," Wiley-Interscience, A Division of John Wiley & Sons, Inc. New York, NY.

Bradshaw, P., 1969, "The Analogy Between Streamline Curvature and Buoyancy in Turbulent Shear Flow," *J. Fluid Mech.*, Vol. 36, p. 177.

Brodkey, R. S., Wallace, J. M. and Eckelmann, H., 1974, "Some Properties of Truncated Turbulence Signals in Bounded Shear Flows," *J. Fluid Mech.*, Vol. 63, p. 209.

Durst, F., Melling, A and Whitelaw, J. H., 1976, "Principles and Practice of Laser Doppler Anemometry," *Academic Press*.

Ellis, L. B. and Joubert, P. N., 1974, "Turbulent Shear Flow in a Curved Duct," *J. Fluid Mech.*, Vol. 62, p. 65.

Eskinazi, S. and Yeh, H., 1956, "An Investigation on Fully Developed Turbulent Flows in a Curved Channel," *J. Aero. Sci.*, Vol. 23, p. 23.

Gillis, J. C. and Johnston, J. P., 1983, "Turbulent Boundary Layer Flow and Structure on a Convex Wall and Its Redevelopment on a Flat Wall," *J. Fluid Mech.*, Vol. 135, p. 123.

Hoffmann, P. H., Muck, K. C. and Bradshaw, P., 1985, "The Effect of Concave Surface Curvature on Turbulent Boundary Layers," *J. Fluid Mech.*, Vol. 161, p. 371.

Hunt, I. A. and Joubert, P.N., 1979, "Effects of Small Streamline Curvature on Turbulent Duct Flow," *J. Fluid Mech.*, Vol. 91, p. 633.

Klebanoff, P. S., 1954, "Characteristics of Turbulence in a Boundary Layer with Zero Pressure Gradient," *NASA TN* 3178.

Kline, S. J. and McClintock, F. A., 1953, "Describing Uncertainties in Single-sample Experiments," *Mechanical Engineering*, Vol. 75, p. 3, Jaunary.

Margolis, D. P. and Lumley, J. L., 1965, "Curved Turbulent Mixing Layer," *Phys. of Fluids*, Vol. 8, No. 10, p. 1775.

McLaughlin, D. K. and Tiederman, W. G., 1973, "Biasing Error Correction for Individual Realization of Laser Anemometer Measurements in Turbulent Flow," *Phys. of Fluids*, Vol. 16, No. 12.

Meroney, R. N. and Bradshaw, P., 1975, "Turbulent Boundary Layer Growth over a Longitudinally Curved Surface," *AIAA J.*, Vol. 13, p. 1448.

Muck, K. C., Hoffmann, P. H. and Bradshaw, P., 1985, "The Effect of Convex Surface Curvature on Turbulent Boundary Layers," *J. Fluid Mech.*, Vol. 161, p. 347.

Ramaprian, B. R. and Shivaprasad, B. G., 1978, "The Structure of Turbulent Boundary Layers Along Mildly Curved Surfaces," *J. Fluid Mech.*, Vol. 85, p. 273.

Smits, A. J., Young, S. T. B. and Bradshaw, P., 1979, "The Effect of Short Regions of High Surface Curvature on Turbulent Boundary Layers," *J. Fluids Mech.*, Vol. 94, p. 209.

So, R. M. C. and Mellor, G. L., 1972, "An Experimental Investigation of Turbulent Boundary Layers Along Curved Surfaces," *NASA CR-1940*.

Tanaka, H. and Yabuki, H., 1986, "Laminarization and Reversion to Turbulence of Low Re. Flow Through a Converging to Constant Area Duct," *J. Fluids Eng.*, Vol. 108, p. 325.

Wattendorf, F. L., 1935, "A Study of the Effect of Curvature on Fully Developed Turbulent Flow," *Pro. Roy. Soc.*, A 148, p. 565.

Wilcken, H., 1930, "Effect of Curved Surfaces on Turbulent Boundary Layers," *NASA TT-F-11421*.